Cost on Reliability and Production Loss for Power Converters in the Doubly Fed Induction Generator to Support Modern Grid Codes

Zhou, Dao; Blaabjerg, Frede; Lau, Mogens; Tonnes, Michael

Published in:
Electric Power Components & Systems

DOI (link to publication from Publisher):
10.1080/15325008.2015.1102990

Publication date:
2016

Cost on Reliability and Production Loss for Power Converters in DFIG to Support Modern Grid Codes

Dao Zhou, Frede Blaabjerg, Mogens Lau, and Michael Tonnes

Abstract - As wind farms are normally located in remote areas, many grid codes have been issued especially related to the reactive power support. Although the Doubly-Fed Induction Generator (DFIG) based power converter is able to control the active power and reactive power independently, the effects of providing reactive power on the lifetime of the power converter and the cost-of-energy of the whole system are seldom evaluated, even though it is an important topic. In this paper, the loss models of the DFIG system are established at various conditions of the reactive power injection. If the mission profile is taken into account, the lifespan of the power semiconductors as well as the cost of the reactive power can be calculated. It is concluded that an over-excited reactive power injection significantly reduces the power converter lifetime, only 1/4 of the case that there is no reactive power exchange between the DFIG and the grid. Besides, if the over-excited reactive power is required all year around, the annual loss of energy can reach 2.74% compared to 2.29% at the case of no reactive power injection. Finally, the reactive power effects on the loss dissipation have been verified in a down-scale DFIG test rig.

Key words - Reactive power, Doubly-Fed Induction Generator (DFIG), reliability, cost-of-energy.

I. Introduction

The shortage of fossil energy, air pollution, and global warming are pushing the technology advancement of renewable resources. As one of the most important candidates, the wind power technology has grown rapidly over the past decades all over the world. It still has a priority status in many countries, and therefore the share of wind power in relation to the overall installed capacity is likely to increase steadily. For instance, in Denmark, a country that pioneered this development, the installed wind power has already reached 30% of the whole electrical energy consumption, and it commits that the capacity will approach to 50% by 2020 [1]-[3]. Another perspective in the wind energy progress is that onshore wind farms are moving to offshore wind parks. Due to the rougher weather, higher cost of the offshore maintenance and service, the reliability of the wind turbine system plays an increasing important role, since 20-25 years of expected lifetime is established as a recent industrial standard. According to a German reliability survey of the wind turbine systems [4], among the failure rate distribution of different components, the power electronics converter is one of the components which have the highest failure rate, and thus more and more efforts are being devoted to the reliability assessment. Although various stressors of power semiconductor (e.g. vibration, contaminants and dust, humidity, temperature cycling, etc.) affect the reliability of power device, the temperature cycling takes up more than a half failure [5]. Furthermore, the thermal performance of the power semiconductors (especially the mean junction temperature and the junction temperature fluctuation) is regarded as the two most important reliability assessment indicators [6].

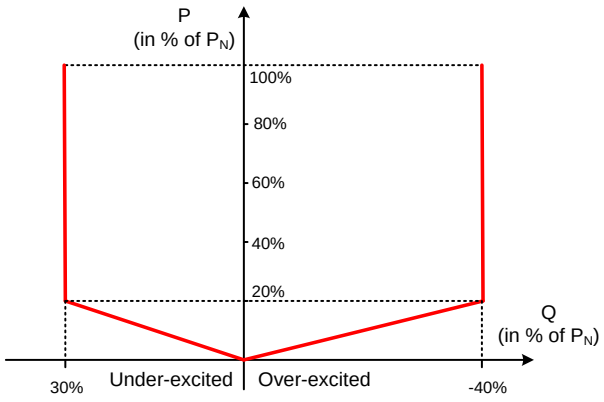

Fig. 1. Reactive power support stated in German grid code [10].

Unlike a conventional synchronous generator, which has the possibility to generate or absorb the reactive power depending on the applied excitation [7]-[9], the increased dominance of the wind turbine system inevitably challenges its role in the provision of the reactive power in order to support the grid voltage. Fig. 1 shows the grid code issued by the German authority E.ON about reactive power requirement [10] – a demand on both under-excited and over-excited reactive power capability even if the grid voltage remains in a normal condition. However, the reactive power capability requires extended design features, which needs a higher initial cost [11]. In other words, if the wind turbine system operates with its original design, it may have higher thermal stress for both the power converters and the generators in order to provide the reactive power. Furthermore, in order to meet the wind energy as an economical affordable form of electricity, the effects of the reactive power on the cost-of-energy is of more and more interest.

An approach of the lifetime estimation is proposed on the basis of mean-time to failure [12], but this concept is not a detailed metrics, since the reliability analysis involves both the mathematics and statistics from the damaged device or the root cause behind the failures. As stated in [13], the thermal cycling of the power converter basically consists of the fundamental frequency caused smaller cycles and the load variation caused larger cycles. Furthermore, the complicated approach based on the mission profile analysis is proposed in [14], in which the long-term, medium-term and short-term characteristics of the annual wind profile are individually studied due to the various time constants of the different components of the wind turbine system. However, this paper reflects the reactive power influence in terms of the lifetime estimation of the power devices as well as cost-of-energy in a Doubly-Fed Induction Generator (DFIG) system, which is able to meet the modern grid codes.

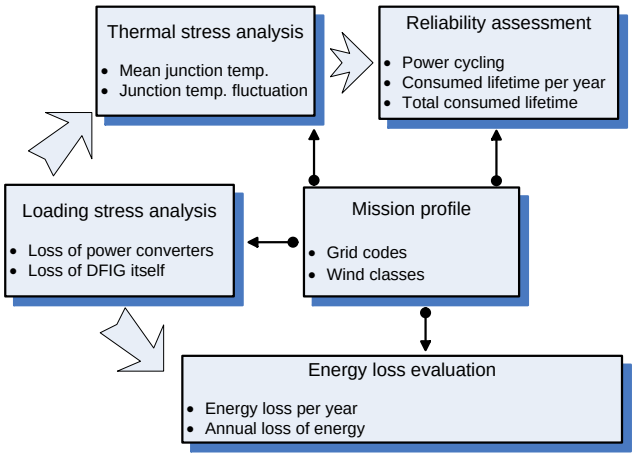

Fig. 2. Flowchart to assess the reliability and energy loss in the DFIG wind turbine system.

The structure of this paper is organized as shown in Fig. 2. In Section II, the additional losses in the back-to-back power converters and the DFIG itself introduced by the reactive power injection is investigated. Section III gives a flowchart to translate the power loss to the power cycles of the power

semiconductors from the thermal stress point of view. Then, the cost of the reactive power on the lifetime of power semiconductor can be analyzed according to an annual wind profile. In Section IV, the cost of the energy production at various types of the reactive power are theoretically evaluated and discussed. The loss of the power converters and the efficiency of the whole DFIG system are experimentally verified in a down-scale DFIG test rig in Section V. Finally, concluding remarks are drawn in Section VI in respect to the reactive power effect on the cost of lifetime as well as the production losses.

II. Evaluation of Loss Profile

DFIG-based wind turbine system is widely used due to its higher efficiency, variable-speed operation, as well as the use of partial-scale power converter that enables independent control of the active power and the reactive power [3], [9], [15]. However, a certain amount of energy is inevitably dissipated from the wind turbine to the power grid, which normally includes the mechanical loss (e.g. drive train loss and gearbox loss) and the electrical loss (e.g. power converters loss and generator loss) [16]. In this paper, only the electrical loss is of interest, and it will be addressed in terms of the back-to-back power converters and the DFIG itself.

A. Loss model of power electronics converters

As shown in Fig. 3, the back-to-back power converters are named as the Rotor-Side Converter (RSC) and the Grid-Side Converter (GSC) due to their positions in the wind turbine system. Both the power converters have two control freedoms – the RSC is allocated to control the stator active power P_s and the reactive power Q_s of the DFIG, while the GSC is designed to keep its active power P_g and reactive power Q_g to the power grid. The reference direction of the power flow is shown in Fig. 3.

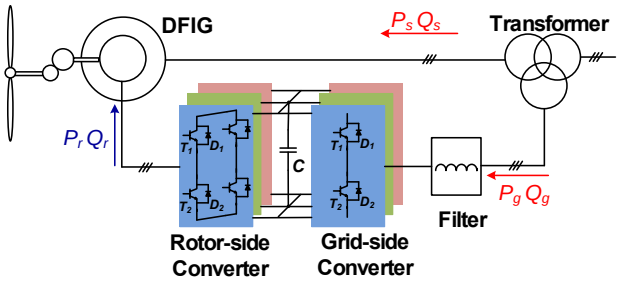

Fig. 3. Configuration of a typical DFIG wind turbine system.

The equivalent circuit model of the DFIG is shown in Fig. 4 represented in d-axis and q-axis [15]. If the stator voltage is oriented for the vector control, neglecting the stator resistor R_s, the rotor resistor R_r, and its equivalent iron loss resistor R_i, the rotor current (transferred to the stator-side) can be calculated as,

$$\begin{cases} i_{rd} = -\dfrac{L_s}{L_m}\dfrac{P_s}{1.5U_s} \\ i_{rq} = (\dfrac{-U_s}{\omega_1 L_m} + \dfrac{L_s}{L_m}\dfrac{Q_s}{1.5U_s}) \end{cases} \quad (1)$$

where U_s denotes the stator voltage, ω_1 denotes the angular frequency of the power grid, P_s and Q_s denote the active power and reactive power defined in Fig. 3. Moreover, L_s and L_m are the stator inductor and magnetizing inductor of the DFIG, respectively. It can be seen that the higher amount of the stator active power causes higher amount of rotor current in the d-axis. Moreover, it is evident that the rotor current in the q-axis is only dependent on the stator reactive power.

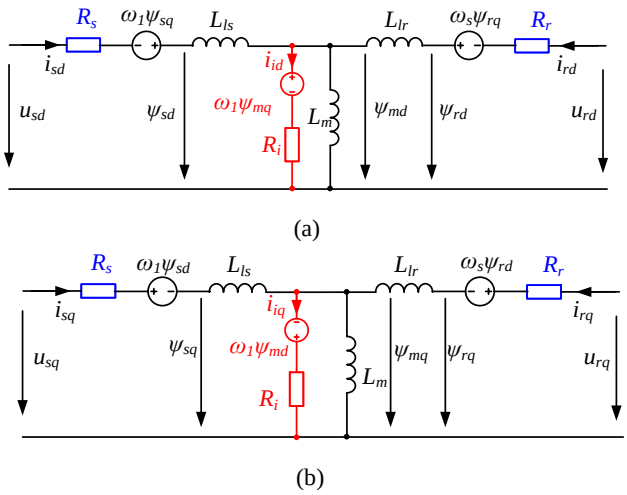

Fig. 4. DFIG equivalent circuit considering the copper loss and the iron loss. (a) d-axis circuit; (b) q-axis circuit.

According to the voltage equation and flux equation indicated in Fig. 4, the rotor voltage (transferred to the stator-side) can be expressed as,

$$\begin{cases} u_{rd} = s(\dfrac{L_r}{L_m}U_s - \dfrac{\sigma L_r L_s \omega_1}{L_m}\dfrac{Q_s}{1.5U_s}) \\ u_{rq} = s\dfrac{\sigma L_r L_s \omega_1}{L_m}\dfrac{P_s}{1.5U_s} \end{cases} \quad (2)$$

where L_r denotes the rotor inductor of the DFIG, s denotes the slip value, and σ is leakage coefficient of the induction generator, defined as $(L_sL_r\text{-}L_m^2)/L_m^2$. It is obvious that the stator reactive power and active power determines the rotor voltage in the dq-axis.

According to (1) and (2), if the rotor current and rotor voltage are transformed back to the rotor-side, the current and the voltage of the RSC can be calculated. It is noted that both the rotor current and the rotor voltage are decided by the active power and the reactive power of the DFIG stator-side.

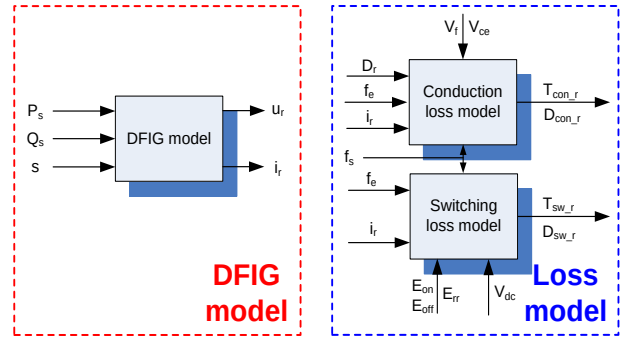

(a)

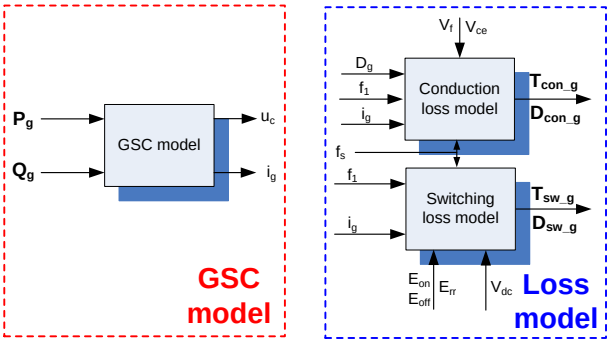

(b)

Fig. 5. Framework to calculate the power loss of power electronics converters. (a) Rotor-side converter; (b) Grid-side converter.

The framework to calculate the power loss of the RSC is shown in Fig. 5(a). It is assumed that the values used from the datasheet operate at maximum junction temperature (150 °C), although these parameters are dependent on the junction temperature. It is known that the loss dissipation of the power switching device mainly consists of the conduction loss and the switching loss [17]. In respect to the conduction loss, due to the symmetrical sequence arrangement in modulation by using the no-zero vector and zero-vector, the duty cycle D_r of each switching period can be obtained according to the phase angle of rotor voltage. Together with the rotor current i_r and voltage drop across the power devices (either V_{ce} of the IGBT or V_f of the diode), the conduction loss of each switching period can be estimated. Besides, the total switching times within a fundamental period is the switching frequency f_s over the fundamental frequency f_e. Finally, the conduction loss (T_{con_r} of the IGBT and D_{con_r} of the diode) can be calculated by the product of the fundamental frequency and the accumulated conduction energy within one fundamental period [18]. Similarly, the switching loss (T_{sw_r} of the IGBT and D_{sw_r} of the diode) is the product of the fundamental frequency and the accumulated switching energy, which is the sum of the turn-on E_{on} and turn-off E_{off} switching energy of the IGBT and the reverse-recovery switching energy E_{rr} of the diode. Furthermore, it is assumed that the switching loss is proportional to the dc-link voltage V_{dc}. It is worth to note that V_{ce}, V_f, E_{on}, E_{off} and E_{rr} are normally tested and provided by manufacturers in their datasheets.

Meanwhile, as the active power flowing through the GSC is the slip power of the DFIG stator-side, the output current of the GSC can be expressed as,

$$\begin{cases} i_{gd} = \dfrac{P_g}{1.5U_g} \\ i_{gq} = -\dfrac{Q_g}{1.5U_g} \end{cases} \tag{3}$$

where U_g denotes the grid voltage, P_g and Q_g denote active power and reactive power defined in Fig. 3.

If a single inductor L_g is used as the grid filter, the output voltage of the GSC in d-axis and q-axis are,

$$\begin{cases} u_{cd} = U_g - \dfrac{\omega_1 L_g Q_g}{1.5U_g} \\ u_{cq} = -\dfrac{\omega_1 L_g P_g}{1.5U_g} \end{cases} \tag{4}$$

According to (3) and (4), it can be seen that the current and voltage of the GSC are both related to its active power and reactive power.

A similar approach can be used to calculate the loss of the GSC. Since the fundamental frequency of the GSC is fixed to grid frequency f_1, the procedure to calculate the GSC power loss is shown in Fig. 5(b).

Although both the RSC and the GSC have the ability to control the reactive power, the RSC is normally regarded as the main component to fulfill the grid codes of the reactive power compensation, because of the stator and rotor winding ratio of the DFIG. As a result, the reactive power injection only affects the power loss of the RSC in the back-to-back power converters. However, if the reactive power is compensated by the RSC, the additional reactive current at the rotor and stator terminal of the DFIG may change the power dissipation of the induction generator.

B. Loss model of DFIG itself

It is known that the power loss of the DFIG itself mainly consists of the copper loss and iron loss. The copper loss P_{cu} is resistive loss occurring in the winding coils and can be calculated using the equivalent dq axis circuit stator resistance R_s and rotor resistance R_r as shown in Fig. 4,

$$P_{cu} = \frac{3}{2} \cdot [(i_{sd}^2 + i_{sq}^2) \cdot R_s + (i_{rd}^2 + i_{rq}^2) \cdot R_r] \tag{5}$$

As mentioned before, both the stator current and rotor current can be expressed in terms of the active power P_s and the reactive power Q_s of the DFIG stator-side.

Generally, the iron loss is produced by the flux change, and it consists of eddy current loss and hysteresis loss, both of which are tightly connected with the operation frequency and flux density [19]. This method needs to know the empirical formula in advance, and the calculation is normally achieved using Finite Element Methods (FEM). Alternatively, the iron loss can be estimated from the electrical point of view [20]-[22], and can be expressed by an equivalent iron resistance R_i in parallel with the magnetizing inductance as shown in Fig. 4.

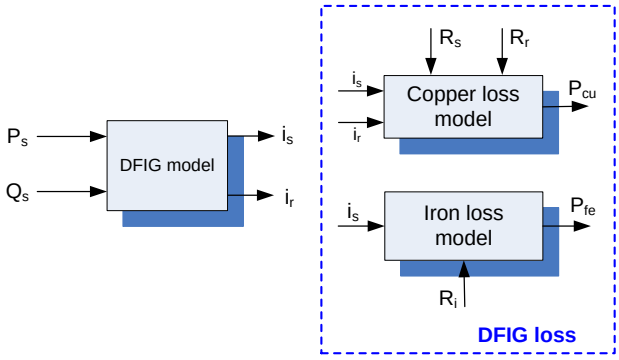

Fig. 6. Framework to calculate the power loss of the DFIG itself.

As the magnetizing flux ψ_m is almost constant during steady-state operation, the voltage equation of the iron loss branch can be simplified as,

$$\begin{cases} R_i \cdot i_{id} = -\omega_1 \cdot \psi_{mq} \\ R_i \cdot i_{iq} = \omega_1 \cdot \psi_{md} \end{cases} \tag{6}$$

where i_i is the current of the iron loss.

With the relationship between the stator flux and the magnetizing flux, the current of the iron loss can be expressed as,

$$\begin{cases} i_{id} = \dfrac{U_s}{R_i} + \dfrac{\omega_1 (L_s - L_m)}{R_i} i_{sq} \\ i_{iq} = -\dfrac{\omega_1 (L_s - L_m)}{R_i} i_{sd} \end{cases} \tag{7}$$

According to (7), the analytical equations of the iron loss current in dq-axis can be achieved. Then, the iron loss P_{fe} can be calculated as,

$$P_{fe} = \frac{3}{2} \cdot [(i_{id}^2 + i_{iq}^2) \cdot R_i] \tag{8}$$

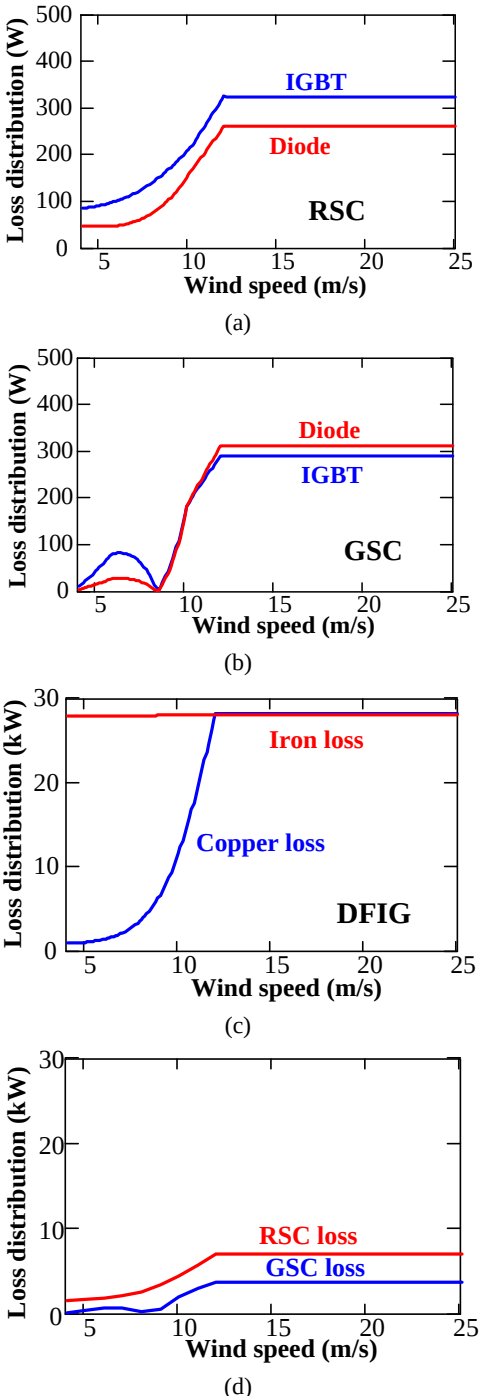

Fig. 7. Loss breakdown of the various parts in the DFIG system. (a) Each power device in the rotor-side converter; (b) Each power device in the grid-side converter; (c) DFIG itself, (d) Rotor-side converter and grid-side converter.

The process to calculate the power loss of the DFIG itself is summarized in Fig. 6, in which the copper loss and the iron loss are taken into account.

C. Loss profile

A 2 MW wind turbine system is used as a case study, and a standard 1 kA/1.7 kV IGBT power module can be used. Due to

the different characteristics of the back-to-back power converters, a single module is used in the GSC arm and two paralleled modules are used in the RSC arm. The wind turbine starts to generate the power from the cut-in wind speed 4 m/s, then the generated power increases with the wind speed using maximum power point tracking until the rated wind speed 12 m/s, finally the rated power is kept from the rated wind speed until the cut-out wind speed 25 m/s.

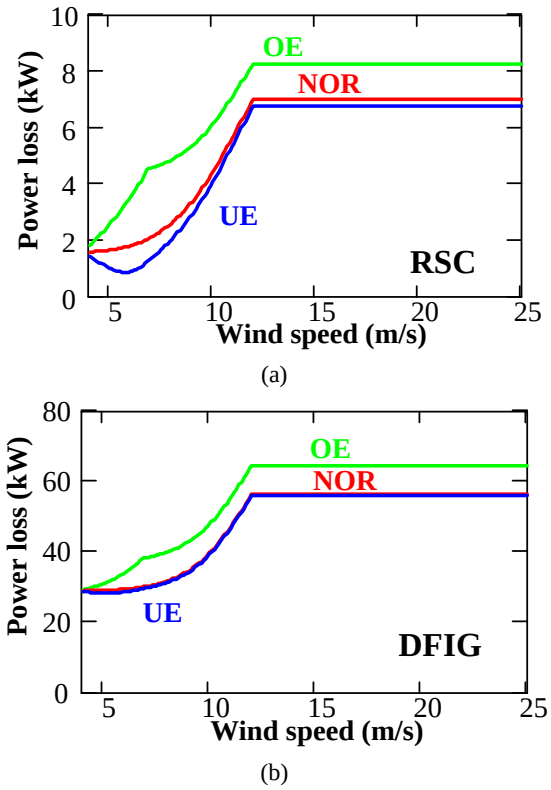

Fig. 8. Reactive power effects on the loss profile. (a) Rotor-side converter; (b) DFIG itself. (OE: over-excited reactive power; NOR: no reactive power; UE: under-excited reactive power).

With the parameters of the DFIG system listed in Appendix, the loss breakdown of the various parts is shown in Fig. 7. For each power device in the RSC, it is noted that both the IGBT and the diode are more loaded with higher wind speed before the wind speed reaches the rated value, and the IGBT is the most stressed compared to the diode. For each power device in the GSC, the minimum power loss appears around the synchronous operation of the DFIG, because the low slip value causes a small power through the GSC. Besides, it is noted that the diode is the most stressed. Compared with the RSC and the GSC, similar loading of the most stressed power semiconductor can be observed. In respect to the DFIG itself, it can be seen that the copper loss increases with the higher wind speed, while the iron loss stays almost constant at different wind speeds. In addition, the copper loss and the iron loss become nearly the same if the wind speed is above the rated value.

As the reactive power compensated from the RSC affects the loading of the RSC and the DFIG itself, Fig. 8 shows the reactive power influence on the loss profile in terms of the Over-Excited reactive power injection (OE), Normal operation (NOR) and Under-Excited reactive power injection (UE). It should be noted that the power loss indicates the whole loss of the RSC as shown in Fig. 8(a). Moreover, it is observed that the OE reactive power significantly increases the loss dissipation, while the UE reactive power decreases the loss dissipation slightly. It is because in the case of the UE reactive power operation, the DFIG is externally excited by the power grid, which reduces the excitation energy that originally comes from the RSC. This also gives the loss profile of the DFIG as shown in Fig. 8(b). Compared with the loss dissipation of the RSC and the DFIG, the DFIG has a much higher power loading.

III. Cost of Reactive Power on Reliability

This section starts with a general method to estimate the lifetime of the power semiconductor. Then, based on an annual wind profile, the cost of the reactive power injection required by the grid codes is analyzed.

A. *Analysis of thermal cycling*

As mentioned before, the thermal dynamics of the power device are the most important parameters in terms of reliability assessment. The thermal impedance that decides the junction temperature of the power device mainly consists of the power module itself (from junction to case), the thermal interface material and the cooling method. It can be given by either a Cauer structure (physical model) or a Foster structure (mathematical model). The thermal impedance of the power module is usually given by the manufacturer, and the value is provided in terms of the multi-layer Foster structure. As the cooling methods are custom-oriented, the thermal impedance of the heat-sink is normally provided by the cooling manufacturer.

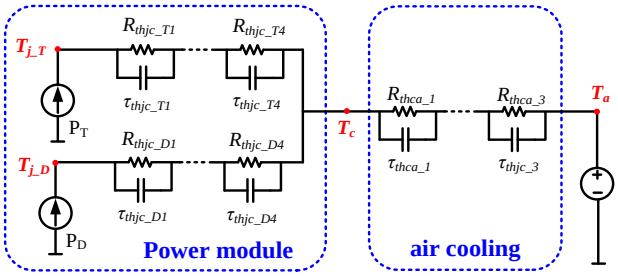

Fig. 9. Thermal model of the power semiconductor for power cycles induced by the fundamental frequency.

Fig. 9 shows a thermal model that combines thermal impedance of the power module and the cooling approach. Generally, the typical thermal time constant of the air cooling is from dozens of seconds to hundreds of seconds for a MW power converter, while the maximum thermal time constant of

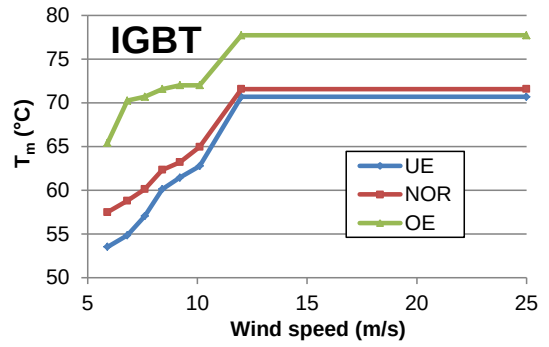

(a)

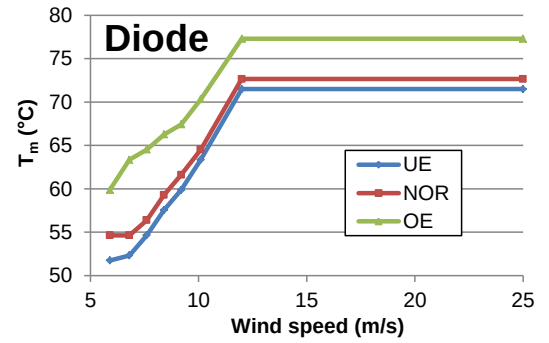

(b)

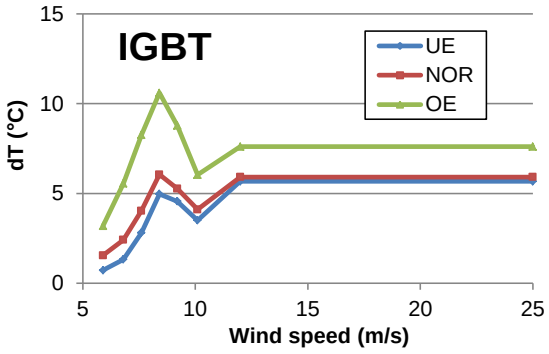

(c)

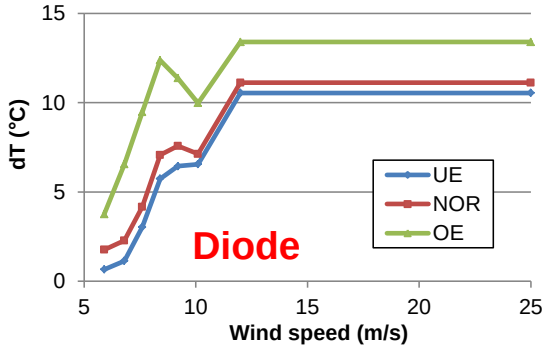

(d)

Fig. 10. Thermal profile of power semiconductors in the rotor-side converter. (a) Mean junction temperature of the IGBT; (b) Mean junction temperature of the diode; (c) Junction temperature fluctuation of the IGBT; (d) Junction temperature fluctuation of the diode.

power module is only hundreds of milliseconds. Moreover, the maximum fundamental period of the power converter current is only several seconds, which implies that the thermal cycling induced by the air cooling can almost be neglected [23], [24]. As a result, the thermal model of cooling will only affect the mean junction temperature, but have no influence on the junction temperature fluctuation.

For the mean junction temperature T_{jm}, it is decided by the thermal resistance of the entire thermal chain [23],

$$T_{jm\_T/D} = P \cdot \sum_{i=1}^{4} R_{thjc\_T/D(i)} + P \cdot \sum_{j=1}^{3} R_{thca\_(j)} + T_a \qquad (9)$$

where R_{thjc} is the thermal resistance from the junction to case, R_{thca} is the thermal resistance of the air cooling. Subscripts T and D denote the IGBT and the freewheeling diode, whereas subscripts i and j mean four-layer and three-layer Foster structure for the power module and air cooling, respectively. P is the power loss of each power semiconductor, and T_a is the ambient temperature of 50 °C.

For the junction temperature fluctuation dT_j, the analytical formula is [23],

$$dT_{j\_T/D} = 2P \cdot \sum_{i=1}^{4} R_{thjc\_T/D(i)} \cdot \frac{(1-\exp(-\frac{t_{on}}{\tau_{thjc\_T/D(i)}}))^2}{1-\exp(-\frac{t_p}{\tau_{thjc\_T/D(i)}})} \qquad (10)$$

where t_p denotes the fundamental period of converter current, t_{on} denotes the on-state time within each fundamental period of current at steady-state operation, τ denotes the each Foster layer's thermal time constant.

The thermal profile of the RSC is shown in Fig. 10(a) and Fig. 10(b) in terms of the mean junction temperature and the junction temperature fluctuation. It can be seen that the tendency of the mean junction temperature is the same with the loss profile, while the junction temperature fluctuation becomes critical around the synchronous operation due to its low operational frequency. Around wind speed of 10 m/s, the turbine reaches the maximum rotational speed, which results in the constant rotor speed of the DFIG. As a consequence, the junction temperature fluctuation starts to increase until the rated wind speed 12 m/s, due to its higher generated electric power.

B. Lifetime model of the power semiconductor

In order to estimate the numbers of power cycles, which the power semiconductor is able to sustain throughout its whole lifespan, the Coffin-Manson lifetime model is used [25],

$$N = A \cdot dT_j^{\alpha} \cdot \exp(\frac{E_a}{k_b \cdot T_{jm}}) \cdot (\frac{t_{on}}{t_{on\_test}})^{\beta} \qquad (11)$$

where E_a and k_b denote the activation energy and Boltzmann constant, respectively. α and A are the constants obtained from LESIT project [25]. It can be seen that the power cycles of the power semiconductor are closely related to the junction temperature fluctuation dT_j and the mean junction temperature T_{jm}. Moreover, the on-state time within each fundamental period of current t_{on} is also relevant to the power cycle capability [6]. Since the power cycles are typically tested at certain on-state time t_{on_test}, and it should be adjusted by a factor of β in order to take the real on-state time of the various operations into account [6], [25].

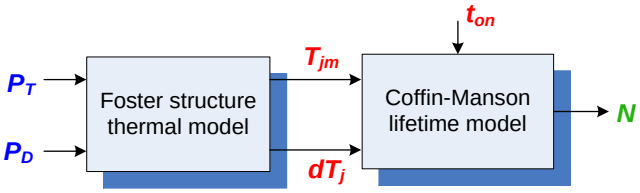

Fig. 11. Framework to estimate the power cycles of the power semiconductors.

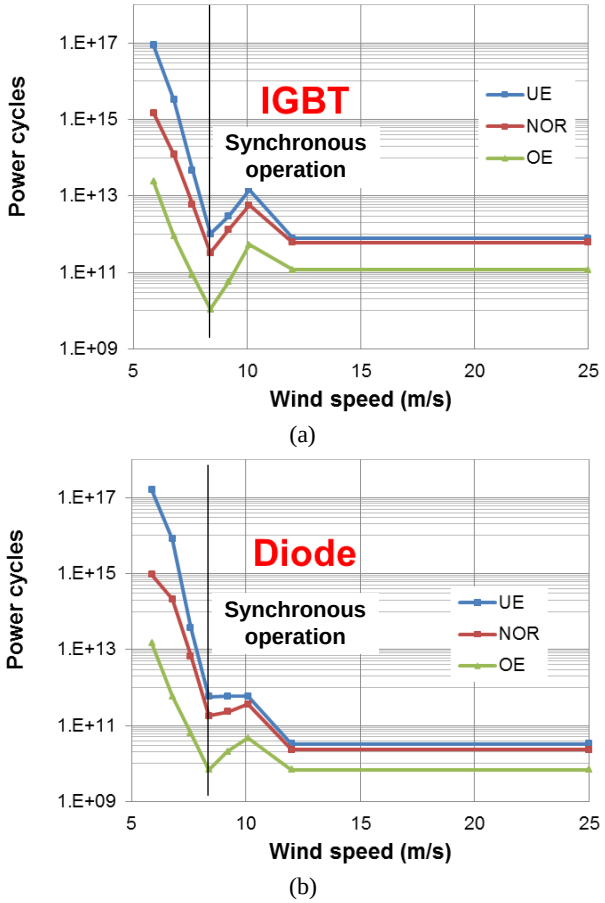

Fig. 12. Power cycles of the power device in the rotor-side converter with various wind speeds. (a) IGBT; (b) Diode.

The procedure to estimate the power cycles of the power semiconductors is shown in Fig. 11. As the RSC is the main converter to meet the reactive power requirement, only the power cycling of the RSC is taken into account. Due to the various thermal performances of the IGBT and the diode, the power cycle curves at different wind speeds are shown in Fig. 12(a) and Fig. 12(b), respectively. It can be seen that the synchronous operation has a very low power cycles due to the high junction temperature fluctuation which is also consistent with Fig. 10(b). Moreover, it can be concluded that the diode almost has lower power cycles compared to the IGBT within the entire wind speed range, so only the reliability of the diode is focused on in this paper, as it is the most loaded device.

C. Method to estimate lifetime

The wind class where the wind turbines are located is one of the important factors which need to be considered during the complex process of planning a wind power plant. It is mainly defined by the average annual wind speed, the speed of the extreme wind gust that could occur over 50 years, and how much turbulence exists at the wind site [26], [27]. According to the IEC standard [26], Class I - high, Class II - medium and Class III - low wind class are defined with annual average speeds of 10 m/s, 8.5 m/s and 7.5 m/s, respectively. Fig. 13 shows an example using the Weibull function to describe the wind distribution, where the region I, II, III and IV are divided by the cut-in, rated and cut-out wind speeds.

Then, the Consumed Lifetime per year (CL) caused by individual wind speed can be defined as,

$$CL_n = D_n \cdot \frac{365 \cdot 24 \cdot 3600 \cdot f_n}{N_n} \tag{12}$$

where D is the percentage of wind speed, f is the fundamental frequency of the converter current, and N is the power cycles calculated by (11). Subscript n denotes the various wind speed from cut-in wind speed 4 m/s to cut-out wind speed 25 m/s, with 1 m/s increment.

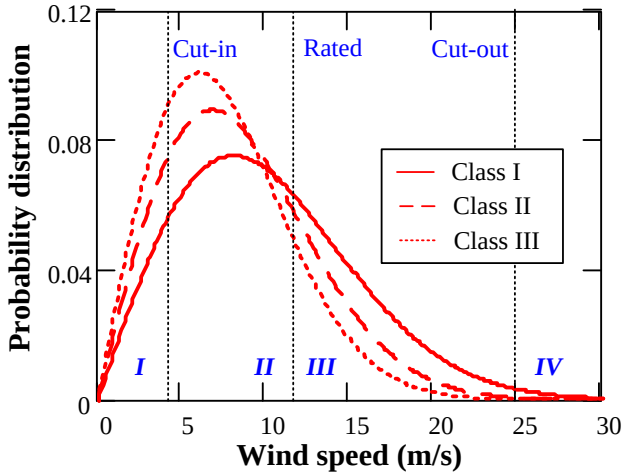

Fig. 13. Annual wind speed distribution according to IEC standard [26].

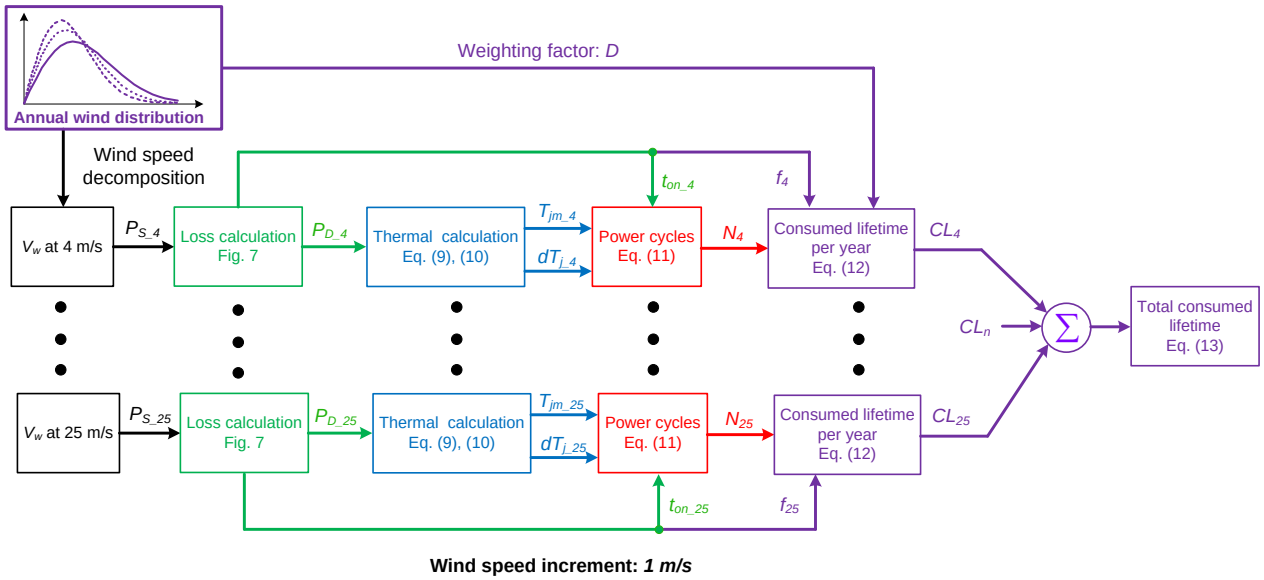

Fig. 14. Block diagram to calculate lifetime based on an annual wind profile for different wind classes.

The Total Consumed Lifetime (TCL) can thus be deduced by summing up all individual consumed lifetimes,

$$TCL = \sum_{n=4}^{25} CL_n \tag{13}$$

The block diagram to calculate the lifetime is shown in Fig. 14. As a result, the lifespan of the power semiconductor can be obtained by the reciprocal of the total consumed lifetime.

D. Reactive power effect on lifetime

If the different types of reactive power (UE, NOR and OE) are required by the transmission system operator, the cost of the reactive power on the lifetime of the diode chip is shown in Fig. 15.

As shown in Fig. 15(a), it is obvious that the OE operation significantly reduces the lifetime of the diode compared to the NOR operation, while the UE operation enhances slightly. Moreover, it is noted that the wind speed at 12 m/s consumes the highest lifetime regardless of the operation modes of the reactive power. The reason is that the rated wind speed has minimum power cycles over the whole speed range seen from Fig. 12(b), and the 12 m/s has highest percentage above the rated wind speed shown in Fig. 13. The total consumed lifetime of the diode at various reactive power injections are summarized in Fig. 15(b). It is noted that the OE operation will shorten the lifetime substantially, almost 1/4 of the NOR operation.

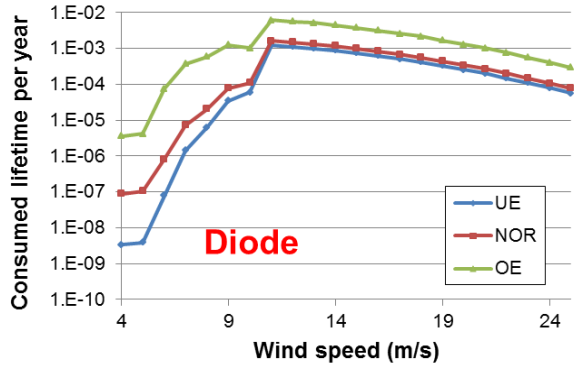

(a)

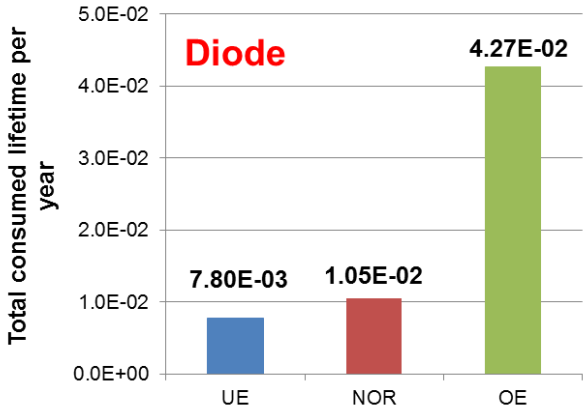

(b)

Fig. 15. Cost of the reactive power on the lifetime of the diode in the rotor-side converter. (a) Consumed lifetime per year; (b) Total consumed lifetime.

IV. Reactive Power Effect On Cost-of-Energy

The cost-of-energy (typically Euro/kWh) generated by different energy resources is the cost to produce electricity at the point of connection to a load or to the grid [28]. It is related to the initial capital cost, operational cost, fuel cost and maintenance, as well as the lifetime expectancy of the whole system. This section will discuss the additional energy loss induced by the reactive power injection, and thereby the cost of the reactive power support can be calculated.

A. *Important concepts*

Based on the loss distribution of the DFIG itself and the power converters described in Section II, together with the annual wind profile, the Energy Loss Per Year (ELPY – unit: MWh) can be calculated by,

$$ELPY = \sum_{n=4}^{12} (P_{RSC\_n} + P_{GSC\_n} + P_{DFIG\_n}) \cdot 365 \cdot 24 \cdot D_n \qquad (14)$$

where P_{RSC}, P_{RSC} and P_{DFIG} represents the loss dissipated of the GSC, RSC and DFIG, respectively. It is noted that the ELPY is only of interest from the cut-in to the rated wind speed, because if the wind speed is higher than the rated value, the power loss dissipated in the DFIG system can be compensated from the mechanical power from the wind turbine blades.

In order to calculate the Annual Energy Production (AEP – unit: MWh), the concerned wind speed is from the cut-in to cut-out wind speed, and the AEP can be obtained by the product of the produced power P_s and the annual wind speed distribution,

$$AEP = \sum_{n=4}^{25} P_{s\_n} \cdot 365 \cdot 24 \cdot D_n \qquad (15)$$

The Annual Loss Of Energy (ALOE – unit: %) can be deduced by dividing the ELPY from the AEP.

$$ALOE = \frac{ELPY}{AEP} \cdot 100\% \qquad (16)$$

As a result, Fig. 16 graphically shows the framework to predict the cost of energy loss in terms of the ELPY, AEP and ALOE for the different operational modes.

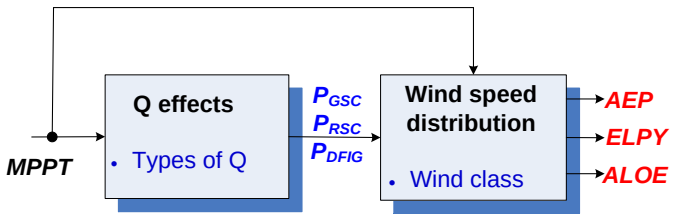

Fig. 16. Framework to predict the cost-of-energy in respect to the reactive power requirement by the grid codes.

B. *Reactive power effects on cost-of-energy*

The ELPY of the DFIG system is shown in Fig. 17(a) in terms of the various types of the reactive power. It is evident that the DFIG itself dominates the energy loss, and the OE operation increases the loss significantly, while the UE operation reduces the loss slightly for both the DFIG itself and the power converters. Moreover, it can be seen that the annual consumed energy loss for a 2 MW turbine is around 217.4 MWh at normal operation.

In respect to the ALOE, it can be seen that nearly 2.29% of the total energy is consumed during the NOR operation. However, up to 2.74% energy is consumed by the DFIG and its power converter in the case of the OE reactive power is provided all year around.

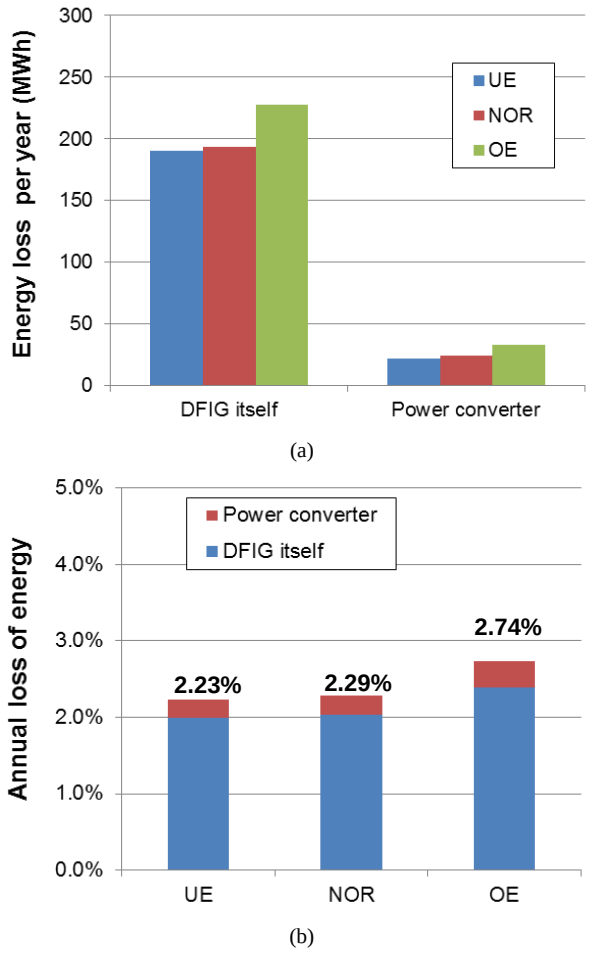

Fig. 17. Reactive power effects on the cost-of-energy. (a) Energy loss per year (ELPY); (b) Annual loss of energy (ALOE).

C. *Various wind profiles*

If various wind classes are taken into account, both the ELPY and the ALOE are shown in Fig. 18. Since the higher wind class has a lower percentage of the wind speed below the rated value as shown in Fig. 13, it is found that higher wind class yields lower annual energy loss in Fig. 18(a). As the higher wind class produces more annual energy, it causes lower annual loss of energy in Fig. 18(b). Moreover, the OE reactive

power increases the cost-of-energy regardless of the wind classes.

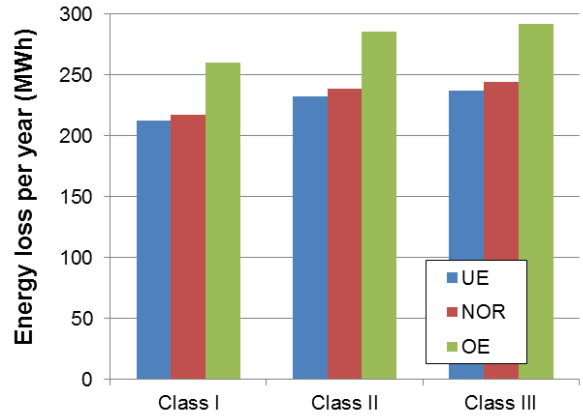

(a)

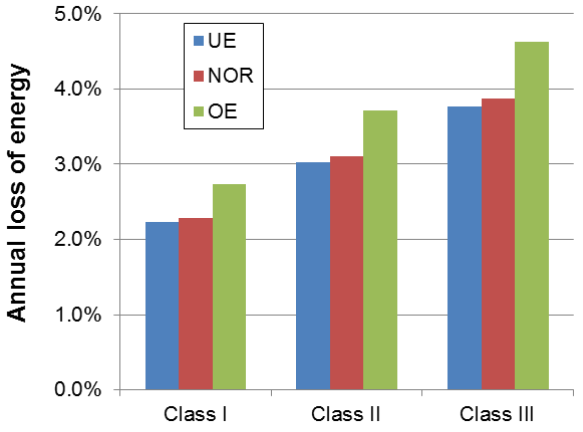

(b)

Fig. 18. Wind class effects on the cost-of-energy. (a) Energy loss per year (ELPY); (b) Annual loss of energy (ALOE).

V. Experimental Validation of Loss Dissipation

According to the previous analysis, the lifetime prediction of the power switching device and the cost of the reactive power are tightly related to the loss profile of the power converters and the DFIG itself. In order to verify the loss model of the power semiconductor and the induction generator, the loss dissipation of the power device and the efficiency of the DFIG system are investigated in a down-scale DFIG system test rig as shown in Fig. 19. A 7.5 kW DFIG is externally driven by a prime motor, and two 5.5 kW motor drives from Danfoss are selected for the GSC and the RSC, both of which are controlled by using dSPACE 1006.

In order to investigate the grid codes influence on the loss dissipation of the power module (both 0.4 pu OE and 0.3 pu UE reactive power as given by grid codes), it is assumed that the DFIG operates at constant speed of 1300 rpm, and the active power varies from 0.2 pu to 1.0 pu. For the GSC, it only deals with the slip power from the generator, and it has a little

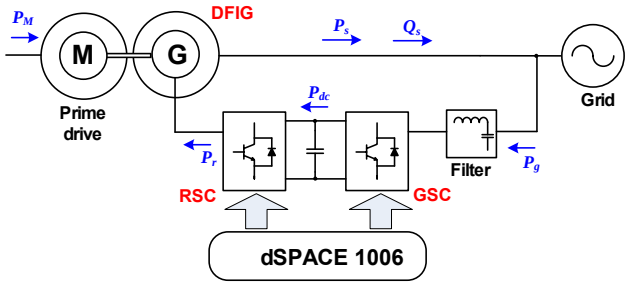

Fig. 19. Setup of the down-scale DFIG system test rig to validate loss modeling.

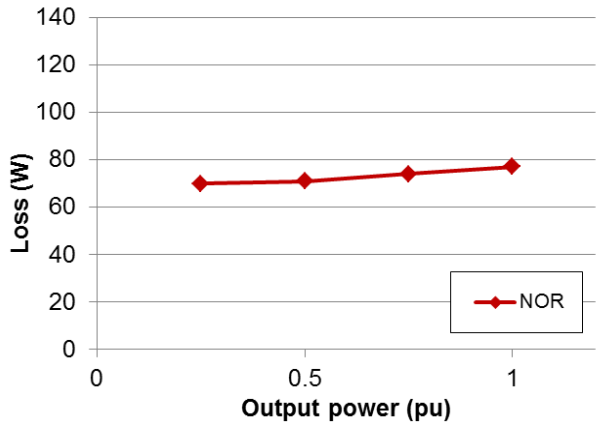

(a)

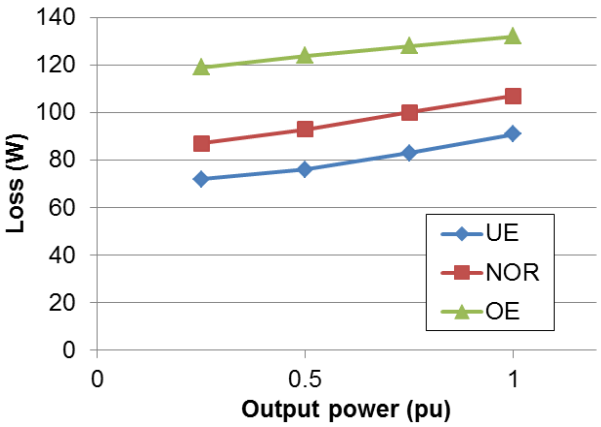

(b)

Fig. 20. Loss dissipation of the DFIG operating at rotor speed of 1300 rpm. (a) Grid-side converter; (b) Rotor-side converter.

responsibility to support the grid codes. It is noted that the loss of the whole power electronics converter is measured by Yokogawa WT3000. As shown in Fig. 20(a), the loss of the GSC increases with the higher output power. For the RSC as shown in Fig. 20(b), similar as the GSC, it is evident that higher output power increases power loss of the RSC. Moreover, it can be seen that the UE reactive power injection decreases the loss dissipation compared to the NOR operation, while the OE

reactive power injection imposes extra loading of the power devices.

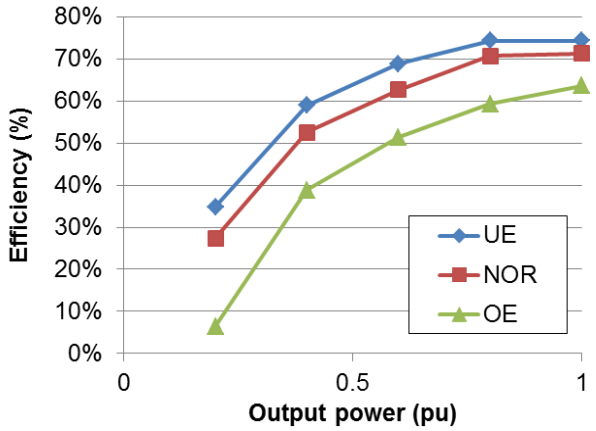

Fig. 21. Efficiency curve for the DFIG test rig at various reactive power injections.

It has been possible to measure the efficiency of the DFIG system including the prime motor. As shown in Fig. 21, the efficiency curve is plotted at various reactive power injections, in which the DFIG operates from 1300 rpm to 1700 rpm with a linear increase of the active power. It is noted that the UE reactive power enhances the efficiency slightly, while the OE reactive power decreases it. Furthermore, due to the loss of the prime motor as well as the much higher value of the stator and the rotor resistance in the down-scale test rig compared to the MW generator listed in Appendix, it can be seen that the efficiency of the whole system becomes low especially at the light loading. However, the characteristics of effects on reactive power injection are the same as the previous loss profile shown in Fig. 8.

VI. Conclusion

In this paper, the effects of the reactive power support on the loss profile of the wind turbine system, lifetime expectancy of the power converter, and the cost-of-energy of the whole system are comprehensively analyzed and evaluated.

Compared with the loss dissipation between the DFIG and its power converters, the DFIG itself consumes more than 80% of the whole power. Moreover, in the case of the over-excited reactive power injection, the loss profile is imposed in both the DFIG itself and the power converters compared to the case when there is no reactive power exchange between the DFIG system and the power grid. However, the injection of the under-excited reactive power decreases the loss profile slightly.

Based on the thermal profile of the power semiconductor, together with a typical annual wind profile, the power cycles can be deduced in terms of the IGBT chip and the diode chip at different wind speeds. It is proven that the diode dominates the lifetime in the rotor-side converter. By the introduction of the consumed lifetime per year and the total consumed lifetime, it is found that the over-excited reactive power significantly reduces the lifetime 1/4 of the normal operation of the most stressed device, which is the diode.

Using the loss profile of the DFIG itself and its power converters, the energy loss per year and the annual loss of energy can be estimated based on the annual wind profile. It is concluded that nearly 2.29% of the total energy is consumed in normal operation, while in the case that the over-excited reactive power is provided all year around, the annual loss of energy increases to 2.74%. Various wind profiles are also taken into account, and it can be seen that higher wind class yields lower annual loss of energy in the same design of the wind turbine system. Finally, the reactive power effects on the loss dissipation of the wind turbine system have been verified in a down-scale DFIG test rig.

Appendix

Parameters Used in 2 MW and 7.5 kW DFIG Wind Turbine Systems

Rated power P_s [kW]	2000	7.5
Rated phase voltage U_s/U_g [V]	690	380
DC-link voltage V_{dc} [V]	1050	650
Stator inductance L_s [pu]	3.891	1.350
Rotor inductance L_r [pu]	3.925	1.378
Magnetizing inductance L_m [pu]	3.840	1.294
Stator resistance R_s [pu]	0.007	0.022
Rotor resistance R_r [pu]	0.006	0.033
Equivalent iron loss resistance R_i [pu]	71.41	35.73
Ratio of stator and rotor winding k	0.369	0.336
Grid filter inductance L_g [pu]	0.660	0.294
Switching frequency f_s [kHz]	2	5

References

[1] Z. Chen, J. M. Guerrero, F. Blaabjerg, "A review of the state of the art of power electronics for wind turbines," *IEEE Trans. on Power Electronics*, vol. 24, no. 8, pp. 1859-1875, Aug. 2009.

[2] F. Blaabjerg, Z. Chen, S. B. Kjaer, "Power electronics as efficient interface in dispersed power generation systems," *IEEE Trans. on Power Electronics*, vol. 19, no. 5, pp. 1184- 1194, Sep. 2004.

[3] M. Liserre, R. Cardenas, M. Molinas, J. Rodriguez, "Overview of multi-MW wind turbines and wind parks," *IEEE Trans. on Industrial Electronics*, vol. 58, no. 4, pp. 1081-1095, Apr. 2011.

[4] B. Hahn, M. Durstewitz, K. Rohrig “Reliability of wind turbines - Experience of 15 years with 1500 WTs,” *Wind Energy: Proceedings of the Euromech Colloquium*, pp. 329-332, Springer-Verlag, Berlin, 2007.

[5] ZVEL, Handbook for robustness validation of automotive electrical/electronic modules, Jun. 2008.

[6] A. Wintrich, U. Nicolai, T. Reimann, “Semikron Application Manual,” pp. 128, 2011.

[7] B. C. Rabelo, W. Hofmann, J. L. da Silva, R. G. de Oliveira, S. R. Silva, "Reactive power control design in doubly fed induction generators for wind turbines," *IEEE Trans. on Industrial Electronics*, vol. 56, no. 10, pp. 4154-4162, Oct. 2009.

[8] M. Z. Sujod, I. Erlich, S. Engelhardt, "Improving the reactive power capability of the DFIG-based wind turbine during operation around the synchronous speed," *IEEE Trans. on Energy Conversion*, vol. 28, no. 3, pp.736-745, Sep. 2013.

[9] S. Foster, L. Xu, B. Fox, "Coordinated reactive power control for facilitating fault ride through of doubly fed induction generator- and fixed speed induction generator-based wind farms," *IET on Renewable Power Generation*, vol. 4, no. 2, pp.128-138, Mar. 2010.

[10] E.ON-Netz. Requirements for offshore grid connections, Apr. 2008.

[11] S. Engelhardt, I. Erlich, C. Feltes, J. Kretschmann, F. Shewarega, "Reactive power capability of wind turbines based on doubly fed induction generators," *IEEE Trans. on Energy Conversion*, vol. 26, no. 1, pp. 364-372, Mar. 2011.

[12] L. Wei, R. J. Kerkman, R. A. Lukaszewski, H. Lu, Z. Yuan, "Analysis of IGBT power cycling capabilities used in doubly fed induction generator wind power system," *IEEE Trans. on Industry Applications*, vol. 47, no. 4, pp. 1794-1801, July-Aug. 2011.

[13] D. Weiss, H. Eckel, “Fundamental frequency and mission profile wearout of IGBT in DFIG converters for windpower”, *in Proc. of EPE 2013*, pp. 1-6, 2013.

[14] K. Ma, M. Liserre, F. Blaabjerg, T. Kerekes, "Thermal loading and lifetime estimation for power device considering mission profiles in wind power converter," *IEEE Trans. on Power Electronics*, vol. 30, no. 2, pp. 590-602, Feb. 2015.

[15] C. Liu, F. Blaabjerg, W. Chen, D. Xu, "Stator current harmonic control with resonant controller for doubly fed induction generator," *IEEE Trans. on Power Electronics*, vol. 27, no. 7, pp. 3207-3220, Jul. 2012.

[16] R. Takahashi, H. Ichita, J. Tamura, M. Kimura, M Ichinose, M. Futami, K. Ide, "Efficiency calculation of wind turbine generation system with doubly-fed induction generator," *in Proc. of International Conference on Electrical Machines (ICEM) 2010*, pp.1-4, 2010.

[17] C. Liu, X. Huang, M. Chen, D. Xu, "Flexible control during grid voltage of DC-link voltage for doubly fed induction generator swell," *in Proc. of ECCE 2010*, pp. 3091-3095, 2010.

[18] D. Zhou, F. Blaabjerg, M. Lau, M. Tonnes, "Optimized reactive power flow of DFIG power converters for better reliability performance considering grid codes," IEEE Trans. on Industrial Electronics, vol. 62, no. 3, pp. 1552-1562, Mar. 2015.

[19] H. Yamaji, T. Shimizu, K. Takano, H. Ishii, "Iron loss evaluation of AC filter inductor core in a PWM inverter," *in Proc. of EPE 2009*, pp.1-8, 2009.

[20] S. Wee, M. Shin, D. Hyun, "Stator-flux-oriented control of induction motor considering iron loss," *IEEE Trans. on Industrial Electronics*, vol. 48, no. 3, pp.602-608, Jun. 2001.

[21] A. G. Abo-Khalil, H. Park, D. Lee, "Loss minimization control for doubly-fed induction generators in variable speed wind turbines," *in Proc. of IECON 2007*, pp.1109-1114, 2007.

[22] B. Chen, T. Lu, Y. Hsu, W. Chen, Z. Lee, "An analytical approach to maximum power tracking and loss minimization of a doubly fed induction generator considering core loss," *IEEE Trans. on Energy Conversion*, vol. 27, no. 2, pp. 449-456, Jun. 2012.

[23] D. Zhou, F. Blaabjerg, M. Lau, M. Tonnes, "Thermal profile analysis of doubly-fed induction generator based wind power converter with air and liquid cooling methods," *in Proc. of EPE 2013*, pp.1-10, 2013.

[24] D. Zhou, F. Blaabjerg, M. Lau, M. Tonnes, “Thermal behavior optimization in multi-MW wind power converter by reactive power circulation,” *IEEE Trans. on Industry Applications*, vol. 50, no. 1, pp. 433-440, Jan. 2014.

[25] R. Amro, J. Lutz, A. Lindemann, "Power cycling with high temperature swing of discrete components based on different technologies," *in Proc. of PESC 2004*, pp. 2593-2598, 2004.

[26] “Wind turbines – part I: design requirements”, IEC 61400-1, 3rd edition.

[27] Vestas website (Available: http://www.vestas.com/en/wind-power-plants/wind-project-planning/siting/wind-classes.aspx?action=3#/vestas-univers)

[28] E. Koutroulis, F. Blaabjerg, "Design optimization of transformerless grid-connected PV inverters including reliability," *IEEE Trans. on Power Electronics*, vol. 28, no. 1, pp.325-335, Jan. 2013.